Electrical Conductivity of Electrospun Polyaniline and Polyaniline-Blend Fibers and Mats

Yuxi Zhang, Gregory C. Rutledge[*]

Department of Chemical Engineering, Massachusetts Institute of Technology, 77 Massachusetts Avenue, Cambridge, MA 02139

ABSTRACT

Submicron fibers of polyaniline (PAni) doped with (+)-camphor-10-sulfonic acid (HCSA) and blended with poly(methyl methacrylate) (PMMA) or poly(ethylene oxide) were electrospun over a range of compositions. Continuous, pure PAni fibers doped with HCSA were also produced by co-axial electrospinning and subsequent removal of the PMMA shell polymer. The electrical conductivities of both the fibers and the mats were characterized. The electrical conductivities of the fibers were found to increase exponentially with the weight percent of doped PAni in the fibers, with values as high as 50 ± 30 S/cm for as-electrospun fibers of 100% doped PAni, and as high as 130 ± 40 S/cm upon further solid state drawing. These high electrical conductivities are attributed to the enhanced molecular orientation arising from extensional deformation in the electrospinning process and afterwards during solid state drawing. A model is proposed that permits the calculation of mat conductivity as a function of fiber conductivity, mat porosity and fiber orientation distribution; the results agree quantitatively with the independently measured mat conductivities.

[*] Corresponding author. Tel.: +1 617 253 0171; fax: +1 617 258 5776. E-mail address: rutledge@mit.edu.

INTRODUCTION

Electrospinning is a convenient method[1] to produce polymer nanofibers with controlled diameters on the order of tens of nanometers to microns.[2] The resulting nonwoven fiber mats have high specific surface areas, around 1 to 100 m^2/g. Combined with the high electrical conductivity of intrinsically conductive polymers, conductive electrospun fiber mats are promising for a variety of applications, such as multifunctional textiles,[3] resistance-based sensors,[4] flexible reversibly hydrophobic surfaces,[5] organic photovoltaics,[6] scaffolds for tissue engineering,[7] and conductive substrates for surface functionalization and modification.[8 9]

Polyaniline (PAni) is one of the most studied electrically conductive polymers, yet it is relatively hard to process compared to most other polymers. As is common among intrinsically conductive polymers, it has a fairly rigid backbone due to the high aromaticity, and is available only in relatively low molecular weight forms, so that the elasticity of its solutions is generally insufficient for it to be electrospun directly into fibers.[10] To circumvent this problem, several different approaches have been reported. Strategies include electrospinning from solutions in concentrated sulfuric acid, a corrosive solvent,[11] coating polyaniline onto a non-conducting substrate,[12] and blending with more flexible, high molecular weight polymers that serve as processing aids.[13 14 15 16 17] However, most of these reports demonstrate only the formation of nanofibers, but do not report their electrical properties. The highest conductivity reported for an electrospun PAni blend fiber is about 1 S/cm.[18] By contrast, conductivities as high as 600 S/cm have been reported for pure polyaniline films and fibers with diameters on the order of hundreds of micrometers.[19] The difference is attributed at least in part to the necessity of blending of PAni with non-conducting polymers in order to form submicron diameter fibers.

While blending high molecular weight non-conducting polymers with the conductive polymers to make the solution electrospinnable remains one of the most effective ways to solve the problem of low

solution elasticity, the resulting fibers have much lower conductivity due to dilution of the conducting component. The co-axial (also known as "two-fluid") electrospinning technique uses two spinnerets that are arranged concentrically so that a low-elasticity fluid introduced to the core of the jet can be elongated along with an electrospinnable fluid introduced to the shell of the jet. The result is a continuous filament with core-shell morphology.[20 21] With the selective removal of the shell component of the resulting fibers, pure component electrospun fibers can be formed from fluids like the pure PAni solutions that are otherwise non-electrospinnable.

In this work, we report the systematic study of conductivities of electrospun fibers of doped PAni blended with different polymers over a range of electrospinnable compositions. Using the co-axial electrospinning method, we produce electrospun fibers of 100% doped PAni, and report their conductivities for the first time. We also report the conductivities of nonwoven mats comprising these fibers, and provide a means for rationalizing the mat conductivities in terms of the mat structure and fiber conductivities.

METHOD

Material

Polyaniline (PAni, emeraldine base, M_w = 65,000) and poly(ethylene oxide) (PEO, M_w = 1,000,000 and 2,000,000 g/mol) were purchased from Sigma-Aldrich, Inc.. The dopant, (+)-camphor-10-sulfonic acid (HCSA), was obtained from Fluka Analytical Chemicals. Poly(methyl methacrylate) (PMMA, M_w = 540,000 and 960,000 g/mol) was purchased from Scientific Polymer Products Inc.. The N,N-dimethylformamide (DMF) and isopropyl alcohol used were OmniSolv® solvents from EMD Chemicals. Chloroform was purchased from Mallinckrodt Chemical Inc. All materials were used without further purification.

Sample Preparation

PAni was dissolved with an equimolar amount of HCSA in chloroform or in a mixture of chloroform and DMF with the weight ratio 5:1 to form solutions with concentrations ranging from 0.5 to 2.0 wt% of doped PAni. PEO or PMMA was then dissolved in these solutions in concentrations ranging from 2.0 to 4.0 wt% to form blended solutions for electrospinning. The parallel-plate electrospinning setup described by Shin et al.[22 23] was used to collect randomly-oriented fiber samples. The plate-to-plate distance was 30 cm. Aligned fiber samples were collected by replacing the lower collection plate with two parallel electrodes to orient the fibers across the gap, as described originally by Li et al.,[24] with the electrodes 4.0 cm apart. The flow rate of the solutions was controlled by a syringe pump (Harvard Apparatus), and varied from 0.015 to 0.05 mL/min. The applied voltage across the plates was varied from 25 to 40 kV. The weight percentage of PAni in the resultant blended fibers ranged from 11% to 67% for the PAni-PEO blend system and 3.8% to 25% for the PAni-PMMA blend system, based on a mass balance of the nonvolatile components in the solutions.

For co-axial electrospinning, the core fluid was 2 wt% PAni with an equimolar amount of HCSA in a 5:1 weight ratio of mixed chloroform and DMF; the shell fluid was 15 wt% PMMA in DMF. The co-axial spinneret had an inner spinneret diameter of 0.46 mm and outer spinneret diameter of 2.03 mm, both of which were charged to the same electrical potential. The core and shell fluid flow rates were 0.01 mL/min and 0.05 mL/min, controlled independently by two syringe pumps. The applied voltage was 34 kV and the distance between the spinneret and collection plate was 30 cm. After the fibers were formed, the resultant fibers and mats were then immersed in isopropyl alcohol for one hour with gentle stirring, so that the PMMA shell component was removed, leaving intact the doped PAni fiber cores.

To increase the molecular orientation within the fibers, the core-shell fibers were post-processed by stretching along the fiber axes. This was achieved by first electrospinning fibers in an oriented fashion between two parallel electrodes connected by an element under compression so that the gap was 1.0 cm, and then partially releasing the compression to realize strains of 0.3 to 1.0.

Characterization

To determine the electrical conductivity of single electrospun fibers, aligned fibers were electrospun in between two parallel electrodes and then deposited onto interdigitated Pt electrodes (IDE, ABTech). The IDEs have 50 sets of interdigitated fingers, and finger width and spacing ranging from 5 to 20μm, as shown in Fig. 1. After deposition, the fiber/IDE sample was hot-pressed at 200ºC and 1 metric ton load for 10 seconds to ensure good electrical contact. A Solartron 1260/1287A high-impedance analyzer was used to measure the resistance between the two electrodes on the IDE. A typical Nyquist plot from the impedance analyzer is shown in Figure 2, where a semicircular trace in the plot shows both resistive and capacitive behavior. The resistance value was read from the Nyquist plot as the extrapolated real-axis (horizontal) intercept at the lowest frequency.

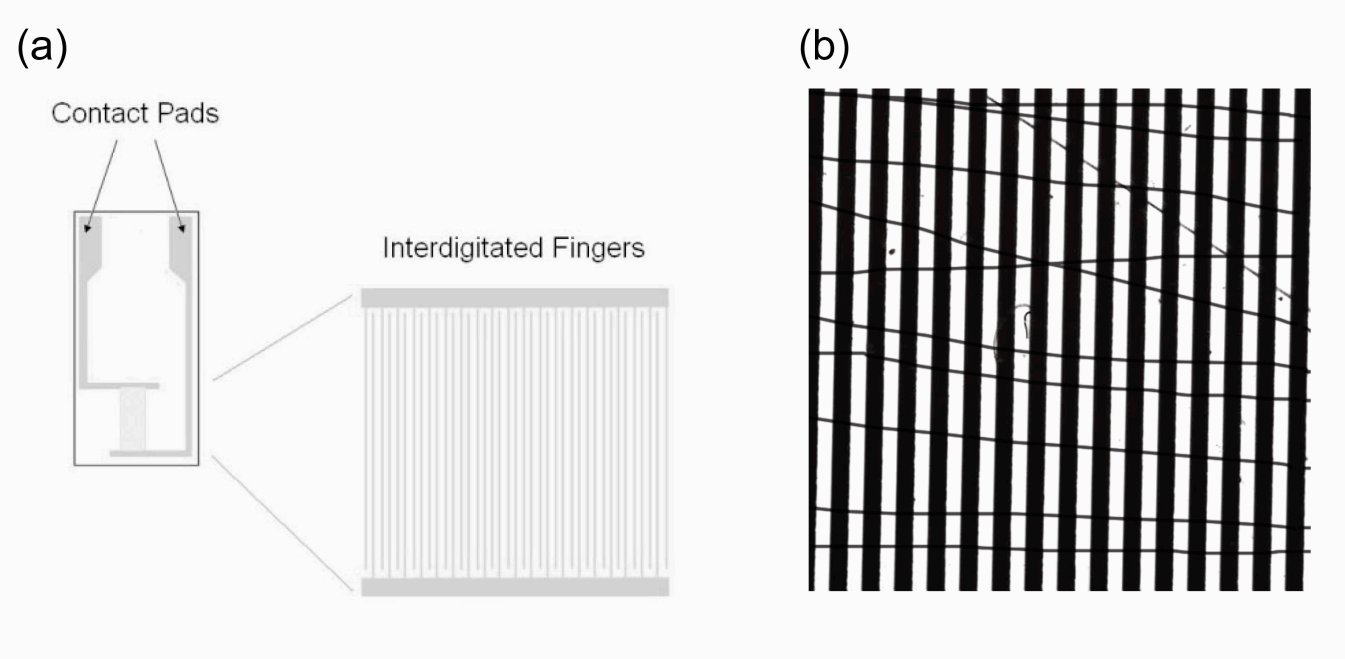

Figure 1 (a) Illustration of the interdigitated electrodes (IDE) and a magnified view of the fingers; (b) optical microscope image of electrospun PAni-PEO blend fibers deposited on IDE and hot-pressed

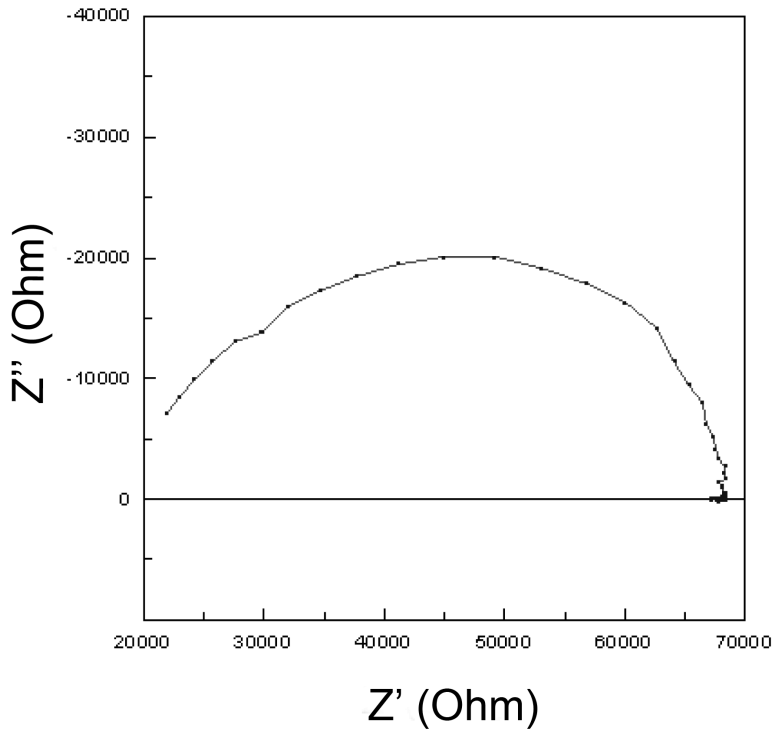

Figure 2 Typical Nyquist plot obtained from the Solartron impedance analyzer for an aligned fiber sample of PAni-PMMA blend fibers with 7.7 wt% of PAni

The average electrical conductivity (σ), which is the inverse of the electical resistivity, can be calculated using Eq, 1, where R is the resistance measured on the IDE, N is the number of parallel pathways formed by fibers on the IDE bridging over the interdigitated fingers (which varies from sample to sample), estimated by optical microscopy (Zeiss Axioskop2 MAT with AxioCam HRc), d is the average fiber diameter obtained by scanning electron microscopy (JOEL JSM-6060) on the as-spun fibers, and δ is the finger spacing (inter-electrode distance) of the IDE:

$$\sigma = \frac{4\delta}{\pi d^2 RN}. \qquad (1)$$

Assuming that the fiber segments act as resistances in parallel, the single-fiber resistance is $R_f = (RN)$. The correction for contact resistance between the fiber and electrode was obtained by measuring the resistance R for N fiber segments deposited under the same processing conditions on IDEs with different finger spacings (5, 10, 15, and 20 μm). Plotting the single-fiber resistance R_f versus the finger spacing and extrapolating the best linear fit (as determined by least squared residuals) to zero finger spacing δ, one obtains the contact resistance, R_{f0}. The uncertainty in R_{f0} was typically less than 20%, which suggests that contact resistance was fairly consistent from sample to sample. This contact resistance was then subtracted from the total resistance to determine the fiber electrical conductivity, according to Eq. 2.

$$\sigma_f = \frac{4\delta}{\pi d^2 \left(R_f - R_{f0}\right)} \qquad (2)$$

Electrical measurements were also performed on both randomly-oriented and aligned electrospun fiber mats. Electrospun fiber mats were cut into rectangular samples that were 2.0 cm in one dimension and various lengths (1.0, 1.5 or 2.0 cm) in the other dimension. The complex resistance between two strips of copper foil placed on the opposing 2.0 cm edges of the mat was measured by the impedance analyzer, so that the spacing between the two copper foils, δ, varied from 1.0 to 1.5 to 2.0 cm. The mat conductivity was calculated based on the geometry of the sample using Eq. 3, where σ_m is the mat conductivity, R is the measured resistance, w is the width of the sample (fixed at 2.0 cm in this study), and t is the thickness of the mat measured by a digital micrometer (Mitutoyo CLM1) with a fixed force of 0.5 N. The contact-resistance was again determined by plotting the measured resistance R versus the electrode spacing, extrapolating the best linear fit (as determined by least squared residuals) to zero electrode spacing, and reading off the contact resistance, R_0. The porosity of the mat, ϕ, was estimated using Eq. 4 by weighing the mass of the mat (m_m) by a digital balance (Caley & Whitmore CP4202S) and using a fiber density value of $\rho_f = 1.0$ g/cm^3. [25]

$$\sigma_m = \frac{\delta}{(R - R_0)wt} \tag{3}$$

$$\phi = 1 - \frac{m_m}{\rho_f \delta w t} \tag{4}$$

Differential scanning calorimetry (DSC, TA Instruments DSC Q1000), and X-ray photoelectron spectroscopy (XPS, Physical Electronics Versaprobe II) were used to characterize the heat capacity and the surface elemental composition of the fibers, respectively.

Polarized Fourier-transformed infrared spectroscopy (polarized-FTIR, Thermo Fisher FTIR6700) was used to measure the molecular orientation of the polyaniline molecules within the electrospun fibers. Bundles of aligned fibers were required for this measurement. The dichloric ratio $D = A_{\parallel} / A_{\perp}$ where $A_{\parallel}$

and $A_{\perp}$ are the absorbance related to the C-N stretching mode (1490 cm^{-1} and 1510 cm^{-1}) measured with the incident beam polarized parallel and perpendicular to the fiber bundle axis, respectively. The overall molecular orientation, f, and the angle between the molecular axis and the fiber bundle axis, Ω, as shown in Fig. 3(a), can be calculated from Eq. 5, [26]

$$f = \frac{3\langle \cos^2 \Omega \rangle - 1}{2} = \frac{(D-1)(2\cot^2 \alpha + 2)}{(D+2)(2\cot^2 \alpha - 1)} \quad , \qquad (5)$$

where α is the angle between the molecular axis and the C-N bonds (shown in Fig. 3(a)). α is between 30º and 39º in polyaniline. Here, $f = 1$ represents perfect alignment of molecules along the fiber axis, $f =$ 0 represents random orientation, and $f = -1/2$ represents molecular alignment perpendicular to the fiber axis.

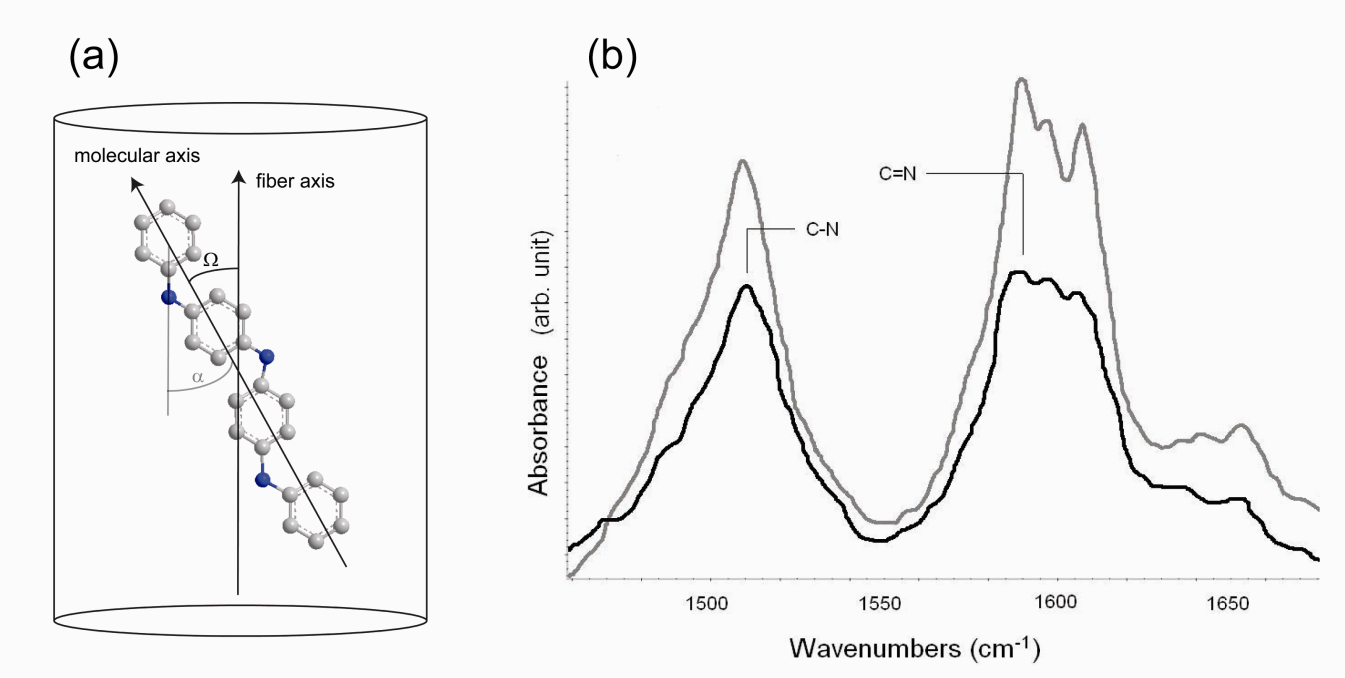

Figure 3 (a) Illustration of molecular orientation of polyaniline in fibers; (b) polarized-FTIR result for PAni fibers stretched to a strain of 0.72, with parallel spectrum in grey and perpendicular spectrum in black

RESULTS AND DISCUSSION

Electrospun Fibers from Blended Solutions

PAni blended with PEO was readily electrospun into fibers from a mixed 5:1 chloroform/DMF solution, with compositions in the range of 11 to 67 wt% PAni in the final fibers. PAni blended with PMMA was electrospun from its chloroform solution to form fibers with 3.8 to 25 wt% PAni in the fibers. Attempts to electrospin blend solutions resulting in higher weight percentage of PAni in the fibers failed to produce continuous fibers, due to insufficient elasticity of the solutions. Detailed processing conditions and resulting fiber electrical conductivities are listed in Table 1. Some typical SEM images of the blended PAni-PEO fibers are shown in Fig. 4.

Table 1 Processing conditions, fiber diameters and electrical conductivities of PAni-blend fibers

Solvent (D: DMF; C: Chloroform)	Blended Polymer & MW	PAni wt% in solution	PAni wt% in resultant fiber	Flowrate (mL/min)	Applied Voltage (kV)	Fiber Diameter (μm)	Fiber Electrical Conductivity (S/cm)
C	PEO, 1M	0.5	11	0.015	35	1.2 ± 0.3	0.02 ± 0.01
C	PEO, 1M	0.5	14	0.015	32	1.6 ± 0.4	0.03 ± 0.02
5:1 C:D	PEO, 1M	1.0	20	0.02	40	1.5 ± 0.3	0.5 ± 0.3
5:1 C:D	PEO, 2M	0.5	33	0.05	35	2.6 ± 0.8	0.8 ± 0.6
5:1 C:D	PEO, 2M	1.0	50	0.05	40	2.7 ± 0.9	2.5 ± 1.5
5:1 C:D	PEO, 2M	2.0	67	0.05	40	2.3 ± 0.7	8.1 ± 3.0
C	PMMA, 0.54M	0.5	3.8	0.05	25	1.6 ± 0.3	$(2.0 \pm 1.0)\times10^{-5}$
C	PMMA, 0.54M	1.0	7.7	0.05	29	1.8 ± 0.3	$(2.8 \pm 1.6)\times10^{-4}$
C	PMMA, 0.54M	1.5	12	0.05	33	1.9 ± 0.4	$(4.0 \pm 1.5)\times10^{-3}$
C	PMMA, 0.96M	1.0	17	0.04	28	1.5 ± 0.2	$(6.5 \pm 3.0)\times10^{-3}$
C	PMMA, 0.96M	1.5	25	0.04	31	1.6 ± 0.3	$(2.3 \pm 1.6)\times10^{-2}$

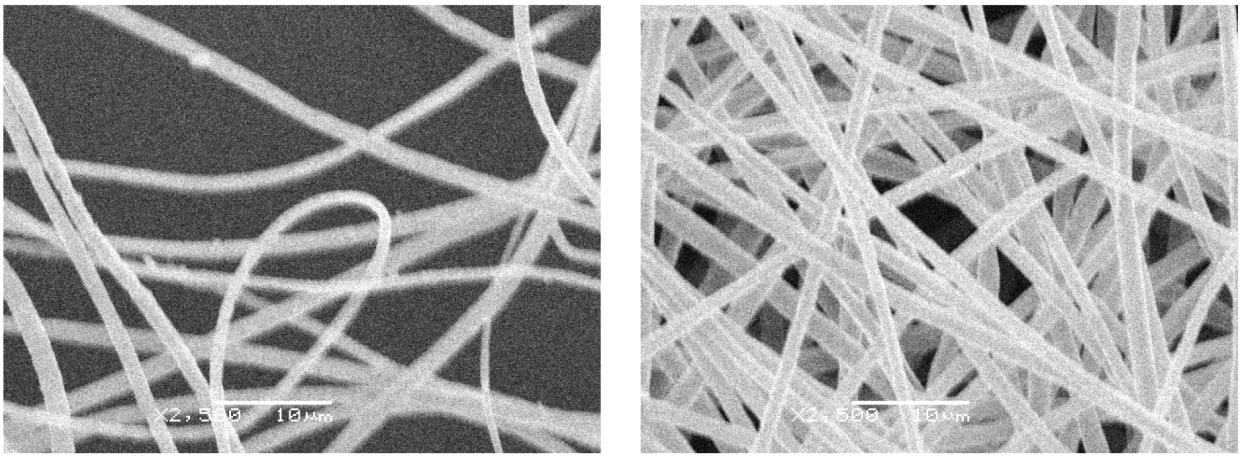

Figure 4 SEM images of PAni-PEO blend electrospun fibers with 11 wt% PAni in blend (left) and 20 wt% PAni in blend (right), PEO M_w = 1,000,000; taken under 2,500× magnification (scale bar = 10 μm)

PAni Fibers from Co-axial Electrospinning

The core-shell PAni-PMMA fibers were fabricated by co-axial electrospinning to achieve smooth and continuous fibers. After removal of the PMMA shell component by isopropyl alcohol, the fiber diameters decreased from 1440 ± 200 to 620 ± 160 nm, but the fiber surfaces were still mostly smooth, as shown by representative SEM images in Fig. 5.

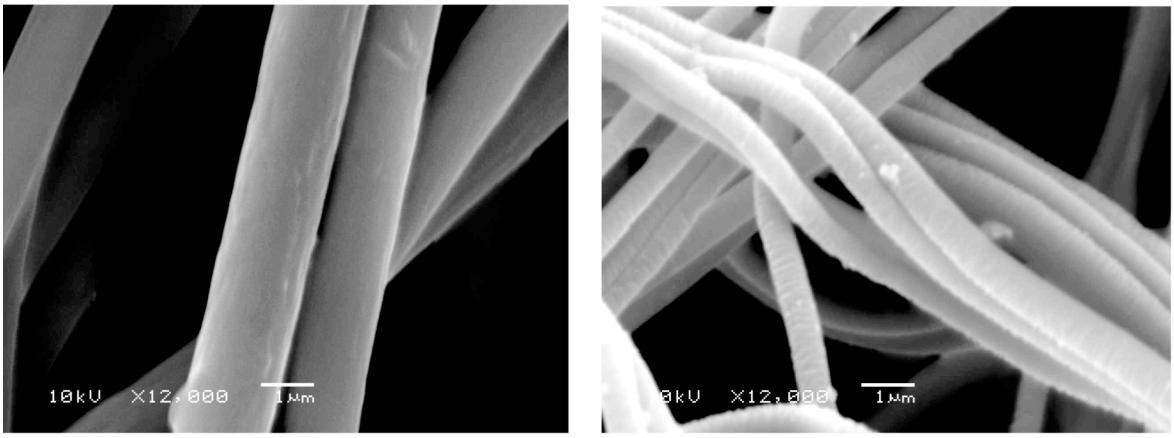

Figure 5 SEM images of electrospun PAni-PMMA core-shell fibers before (left) and after (right) dissolution of PMMA by isopropyl alcohol; taken under 12,000× magnification (scale bar = 1 μm)

X-ray photoelectron spectroscopy (XPS) was used to determine the extent to which the shell component was removed by dissolution in isopropyl alcohol. XPS generally probes only the first (approximately) 10 nm of the surface of the samples, so it provides an accurate measure of the surface composition. As shown in Table 2, the results suggest that before dissolution the surface of the fibers is almost entirely PMMA, while after dissolution most of the PMMA is gone, leaving behind PAni and the dopant HCSA. As the ratio of PAni to HCSA should ideally be 1 to 1 in the fibers, the XPS results suggest that some of the dopant is lost during the dissolution process, and possibly in the electrospinning process itself, too. This contributes negatively to the conductivities measured, as fibers with compositions less than the equimolar amount of dopant to PAni are known to exhibit lower electrical conductivities than those with equimolar amounts of dopant.[27]

Table 2 XPS Results showing Surface Compositions of Core-Shell Electrospun Fibers before and after Dissolution of Shell

	Before Dissolving Shell	After Dissolving Shell
C atomic %	73 ± 2	81 ± 3
O atomic %	26 ± 2	8.7 ± 2.0
N atomic %	0.87 ± 0.10	8.2 ± 0.5
S atomic %	0.03 ± 0.005	2.0 ± 0.2
PAni %	6.5 ± 0.6	67 ± 4
HCSA %	0.6 ± 0.4	30 ± 4
PMMA %	93 ± 3	4.5 ± 2.0

Differential scanning calorimetry (DSC) was also used to characterize the composition of the core-shell fibers measured between -40 and 160 ºC. The results show no discernable PMMA glass transition signals (T_g = 124ºC) in the core-shell PAni fibers after removal of the shell, further supporting the claim that almost all of the PMMA in the shell has been removed. Both PAni and HCSA signals are observed in the fibers separately, suggesting that there is some phase separation between PAni and the dopant HCSA. This also affects the measured conductivities negatively, as phase separation of the two components decreases the electrical conductivity of the system.[27] Also, PAni in this form shows no crystallinity transition between -40 and 160 ºC.

Fiber Electrical Conductivity

The fiber electrical conductivities of the as-electrospun polyaniline and polyaniline-blend fibers are summarized in Fig. 6. These are the results of electrical conductivities measured by IDE across the

whole range of polyaniline compositions in the electrospun fibers, up to 100% for the fibers formed by co-axial electrospinning and subsequent dissolution of the shell.

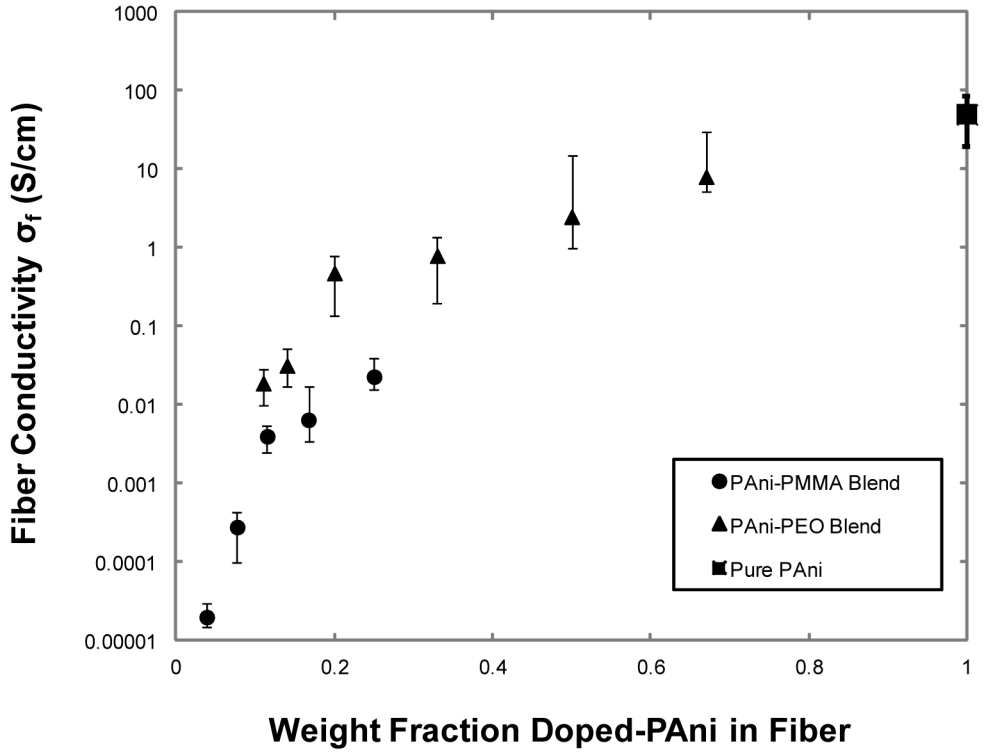

Figure 6 Electrical conductivity of as-electrospun polyaniline fibers (nominally doped with an equimolar amount of HCSA) as a function of the weight fraction of PAni in the blended fibers; the pure PAni fiber was obtained after dissolving the shell component (PMMA) of the core-shell fibers

The electrical conductivity of electrospun polyaniline-blend fibers increases exponentially with the weight percent of doped polyaniline in the fibers. The electrical conductivities of the PAni-PEO blend fibers are an order of magnitude higher than those of the PAni-PMMA blend fibers for the same weight percent of PAni, indicating that the blend polymers are not simply acting as non-conducting fillers in the fibers. The difference in conductivities of the PEO and PMMA blends is attributed to the different intrinsic conductivities of PEO (~10^{-6} S/cm) and PMMA (~10^{-10} S/cm) and the difference in their degree of compatibility with PAni. [12]

The highest electrical conductivity achieved is for the 100% PAni fibers after the shell PMMA component was removed; the calculated fiber conductivity is found to be 50 ± 30 S/cm. To the best of our knowledge, this value is the highest electrical conductivities measured for electrospun polyaniline nanofibers, comparable to that reported by Yu et al.[28] for electrospun fiber bundles.

Solid State Drawing of Electrospun Fibers

In order to increase the electrical conductivities of the PAni fibers, we stretched the core-shell PAni/PMMA fibers along their fiber axes, with strains up to 100%. There was no apparent separation of core and shell layers due to the deformation. The shell component of the stretched fibers was then dissolved by isopropyl alcohol, similar to the as-electrospun fibers, and the fiber conductivities measured. The results are shown in Table 3.

Table 3 Electrical Conductivities of PAni Fibers after Stretching

Strain	Fiber Diameter (nm) after removing shell	Electrical Conductivity (S/cm) after removing shell
0	620 ± 160	50 ± 30
0.30	570 ± 200	54 ± 15
0.50	500 ± 150	70 ± 50
0.72	450 ± 70	105 ± 40
1.0	420 ± 130	130 ± 40

As expected, the fiber diameters decrease with increasing strain. The electrical conductivities, on the other hand, increase noticeably with increasing strain. The highest electrical conductivity achieved this

way was 130 ± 40 S/cm, a three-fold improvement over the as-spun fiber conductivity. Note that all fiber conductivities reported here have been corrected for contact resistance.

To explain the improvement of conductivity with deformation, the results of the polarized FTIR measurements on the stretched fibers are shown in Figure 7. It shows a clear positive correlation between the electrical conductivities and the molecular alignment within the fibers. The as-spun fibers exhibit a modest level of molecular orientation (f = 0.1 - 0.15 for d = 620 nm). This is comparable to the orientation observed by Pai et al in as-electrospun fibers of PA 6(3)T (poly(trimethyl hexamethylene terephthalamide)) of comparable diameter,[29] and can be attributed to the elongational nature of the fiber forming process. Subsequent solid-state drawing increases the molecular orientation to levels (f = 0.35-0.4) previously observed only for as-electrospun PA 6(3)T fibers with diameters on the order of 100 nm. It can thus be concluded that post-spin solid state drawing is more efficient than elongational flows during fiber formation to increase molecular orientation, and that the enhanced molecular orientation is the origin of the higher conductivities observed.

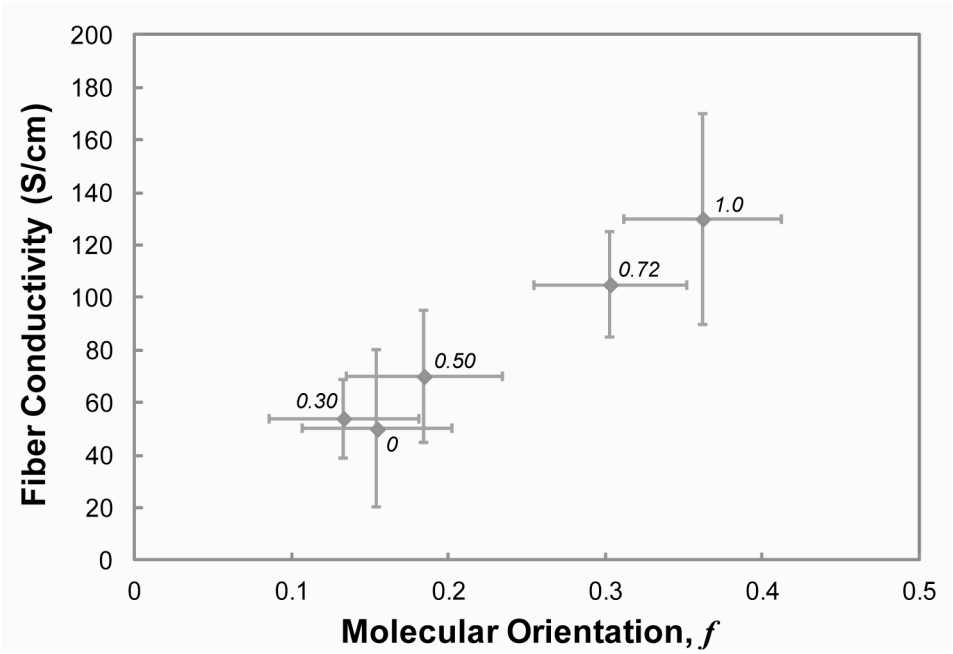

Figure 7 Electrical conductivity of the pure polyaniline fiber, as-spun and after solid-state drawing, as a function of molecular orientation within the fibers, as measured by polarized FTIR from aligned fiber bundles; the label next to each data point shows the corresponding nominal strain from Table 3.

Mat Conductivity

The measured mat conductivities, defined by Eq. 3, are shown in Figure 8. The trend in conductivity of the mats with composition is very similar to that observed for the fibers themselves, shown in Figure 6, but the values are lower by an order of magnitude or more. This difference between the fiber conductivities and mat conductivities can be caused by several factors. These may include differences in fiber composition, fiber microstructure, fiber curl, mat porosity, fiber orientation distribution within mats, fiber-fiber contacts in mats, etc. In order to reconcile these differences, we consider the effect of several of these factors in turn.

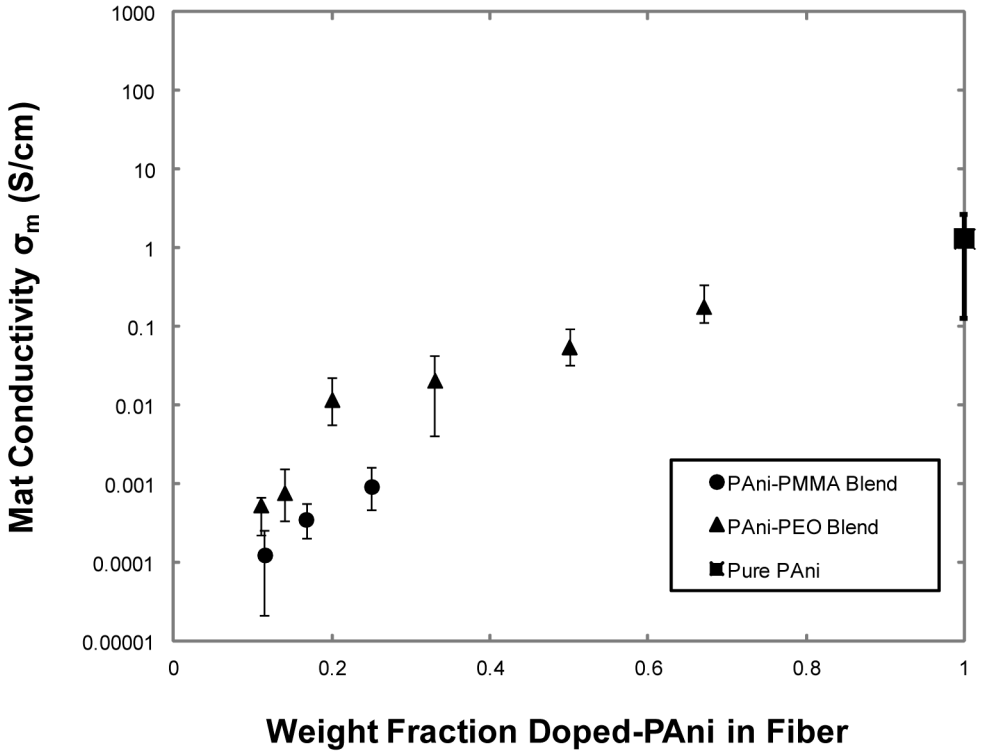

Figure 8 Mat electrical conductivity of polyaniline fiber mats (as-electrospun, nominally doped with an equimolar amount of HCSA) as a function of the PAni weight fraction in the blended fibers; the pure PAni fiber mat was obtained after dissolving the shell component (PMMA) of the core-shell fibers

To account for mat porosity, we adopt a simple, volume-averaged model for mat conductivity based on the rule of mixtures, expressed by Eq. 6, where σ_m^{calc} is the calculated mat conductivity, σ_f is the measured fiber conductivity, and ϕ is the measured mat porosity. The matrix (void) component has effectively zero conductivity, $\sigma_{void}=0$. Variations in composition are taken in to account through the use of the measured fiber conductivity of the same composition; molecular orientation within the fibers is assumed to be comparable for both aligned fibers on IDE's and randomly orientated mats.

$$\sigma_m^{calc} = (1-\phi)\sigma_f + \phi\sigma_{void} = (1-\phi)\sigma_f \qquad (6)$$

Next, we account for the effect of fiber orientation on the measured resistances of the mats. Unlike the measurement of fiber conductivity on the IDEs, where the fibers were collected in an aligned fashion and Eq. 2 can be applied, the measured mat conductivity depends on both the length of the copper foil electrodes and the distance of separation between them. Since nonwoven fiber mats generally do not have a unidirectional aligned fiber orientation distribution, some fraction of the fibers does not provide a conducting path from one electrode to the other; furthermore, those that do provide a conducting path are generally inclined at some angle to the normal direction between electrodes, and so experience a longer path length. To account for this, we assume that all of the fibers act as resistors in parallel. Let the length of individual fiber that connects both electrodes be *l*. The resistance to electrical current from one electrode to the other via this fiber is expressed by Eq. 7,

$$R_f = \frac{4l}{\pi d^2 \sigma_f} \quad . \tag{7}$$

The inverse of total resistance is obtained as the sum of the inverse resistances of all fibers that provide a conducting path from one electrode to the other:

$$\frac{1}{R} = \sum_{i=1}^{N} \frac{1}{R_{f,i}} = \left[\frac{\pi}{4} \sum_{i=1}^{N} \frac{d_i^2 \sigma_{f,i}}{l_i} \right] \quad . \tag{8}$$

Plugging Eq. 8 into Eq. 1, we obtain:

$$\sigma_f^{odf} = \delta \left\langle \sigma_f / l \right\rangle, \tag{9}$$

where the superscript ‘odf’ has been introduced to clarify that the effective fiber conductivity in the two-electrode experiment depends on the orientation distribution function (odf) of the fibers within the mat.

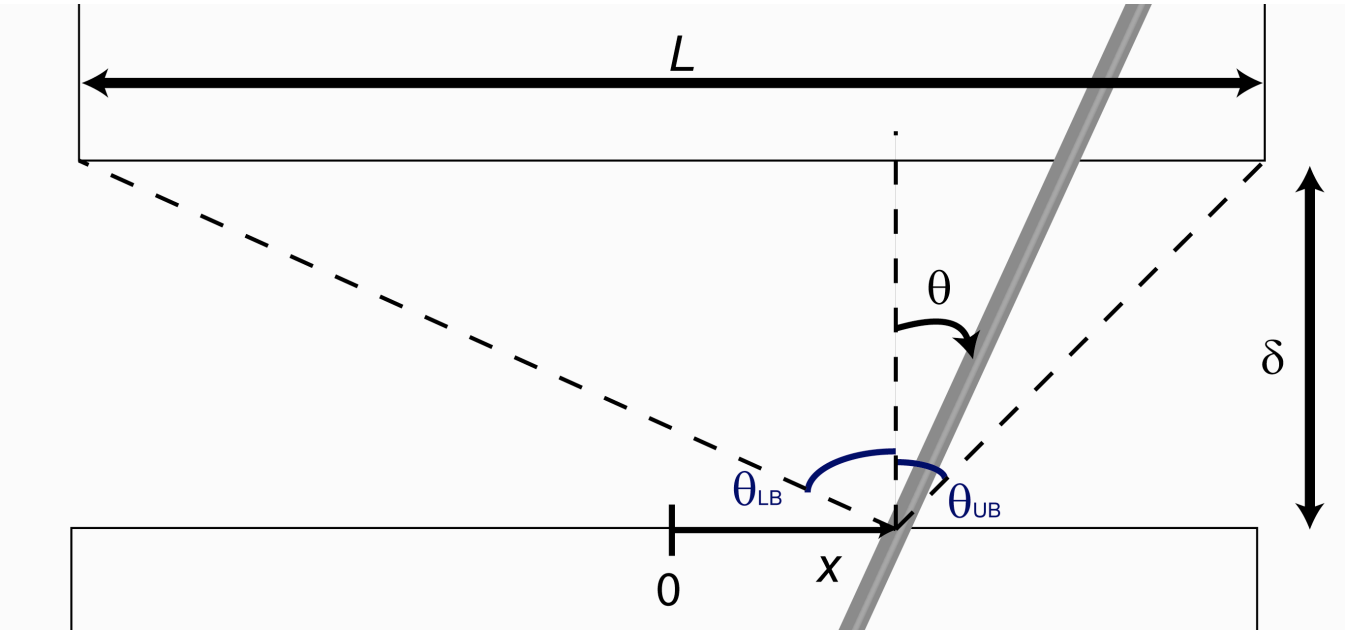

Figure 9 Definition of fiber orientation angle θ between across two electrodes with width *L,* separated by a gap δ. X denotes the position where the fiber makes contact with one of the electrodes. $\theta_{LB}(x)$ and $\theta_{UB}(x)$ denote the upper and lower bounds in orientation angle, beyond which a fiber located at position x does not make contact with the second electrode

To evaluate the fiber ensemble average $\langle \sigma_f / l \rangle$, we sum over all the fibers that contact the first electrode at a point x with an orientation angle θ, as illustrated in Figure 9. The corresponding orientation distribution function is $p(x,\theta)$. We assume that the fiber orientation distribution is uniform throughout the mat and independent of the position x, i.e. $p(x,\theta) = (1/L)p(\theta)$, where L is the length of the copper foil electrodes, and that the fibers are straight, with length $l = \delta/\cos\theta$. The range of orientation angle within which a fiber leaving the first electrode makes contact with the second electrode is a function of position, x. The upper and lower bounds of the range are $\theta_{UB}(x) = \arctan\left(\left(L-2x\right)/2\delta\right)$ and $\theta_{LB}(x) = \arctan\left(\left(-L-2x\right)/2\delta\right)$, respectively. We assume that these fibers all have the same fiber conductivity, as measured by the IDE experiments. Fibers that fall outside of these bounds do not make

contact with the second electrode and have effectively infinite resistance ($\sigma_{f,i} = 0$) for purposes of the mat measurement. This leads to the following expression:

$$\begin{aligned}\sigma_f^{odf} &= \delta \int_{-L/2}^{L/2} dx \int_{-\pi/2}^{\pi/2} \frac{\sigma_f(x,\theta)}{l(x,\theta)} p(x,\theta)\, d\theta \\ &= \frac{\sigma_f}{L} \int_{-L/2}^{L/2} dx \int_{\theta_{LB}(x)}^{\theta_{UB}(x)} p(\theta) \cos\theta \, d\theta\end{aligned} \tag{10}$$

Replacing the fiber conductivity with its odf-corrected value in Eq. 6, we obtain the following relation, which accounts for composition, porosity and fiber orientation distribution within the mat:

$$\sigma_m^{calc} = (1-\phi)\sigma_f^{odf} = (1-\phi)\sigma_f \left(\delta \langle 1/l \rangle\right). \tag{11}$$

To determine the mat conductivity calculated according to this model, we first measured the orientation distribution of fibers in the mats, $p(\theta)$, by SEM image analysis.[30] We then evaluated the double integral of Eq. 10 numerically using the `quad2d` function in MATLAB to obtain the value of the orientation correction factor, $\left(\delta \langle 1/l \rangle\right)$. Figure 10 shows the variation of the orientation correction factor as a function of the ratio of the electrode length to separation, L/δ, for the special case of a random in-plane fiber orientation distribution function, $p(\theta)=1/\pi$.

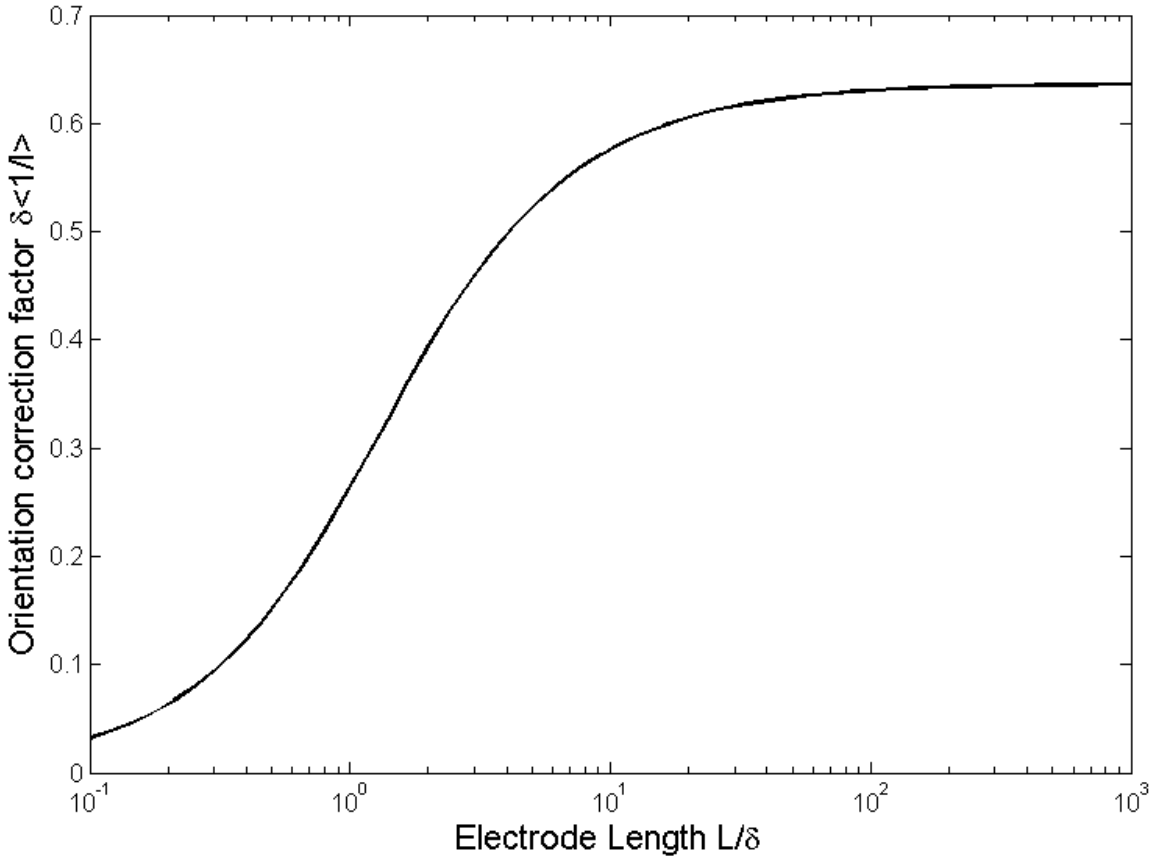

Figure 10 Orientation correction factor for mat conductivity as a function of the measurement geometry (ratio of electrode length to electrode separation), assuming a uniform angular distribution of fibers in the plane of the mat

To check the validity of this orientation correction factor, we fabricated mats with different fiber orientation distributions for each of three different fiber compositions, 20% PAni-PEO, 67% PAni-PEO, and 16% PAni-PMMA. The results for the mats of 20 wt% PAni blended with PEO are shown in Figure 11. The ratio σ_m / σ_f scales almost linearly with the orientation factor. The results for 67% PAni-PEO, and 16% PAni-PMMA showed similar trends. The linearity of this relationship confirms the accuracy of the orientation correction factor expressed by Eq. 10.

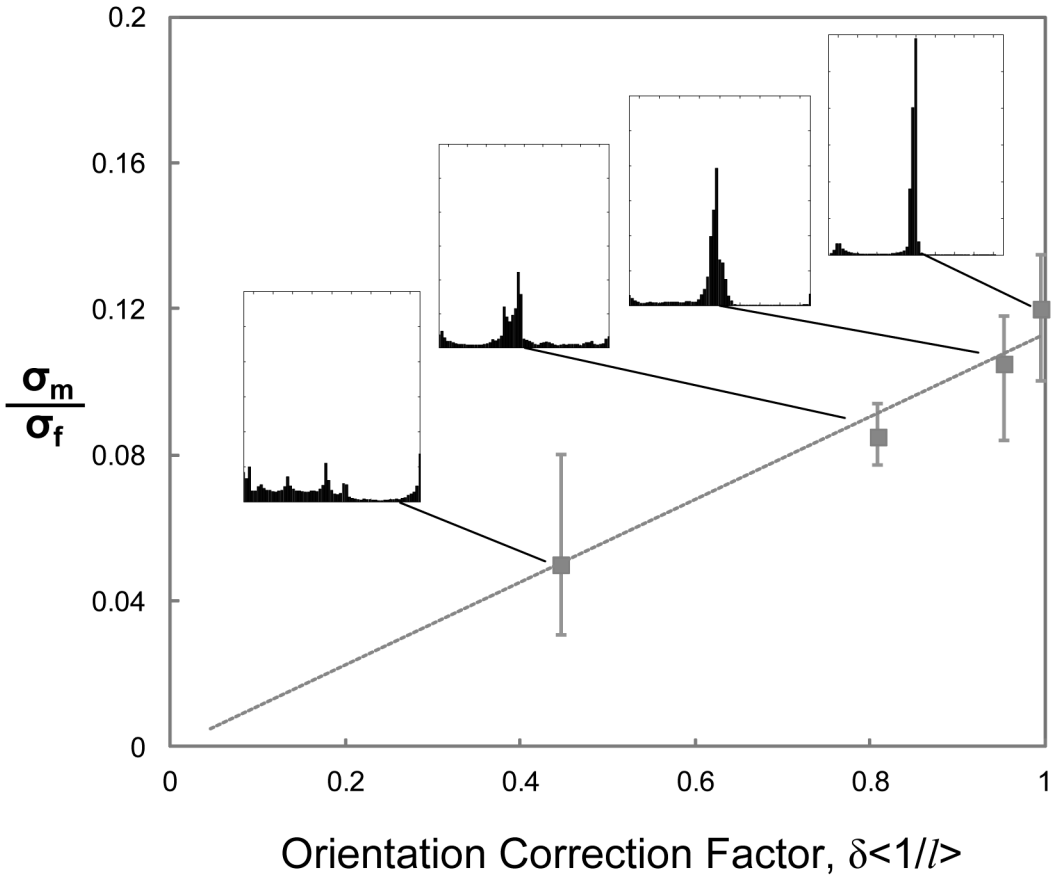

Figure 11 Correlation between dimensionless conductivity ratio (mat to fiber) and orientation distribution of fibers in the mat for samples with 20 wt% PAni blended with PEO. The insets show histograms of the angular orientation distribution for each sample from SEM image analysis. For each inset, the abscissa ranges from -90º to 90º, while the ordinate goes from 0 to 12000 counts

Finally, Figure 12 shows a parity plot of the experimentally-measured mat conductivity versus the mat conductivity predicted by the model for different fiber mat compositions, based on the experimentally-observed fiber conductivity, porosity and fiber orientation distribution according to Eq. 11,. The results

show that the model predicts the mat conductivity quite well, although for most samples the predicted value is slightly higher than the experimentally-measured mat conductivity.

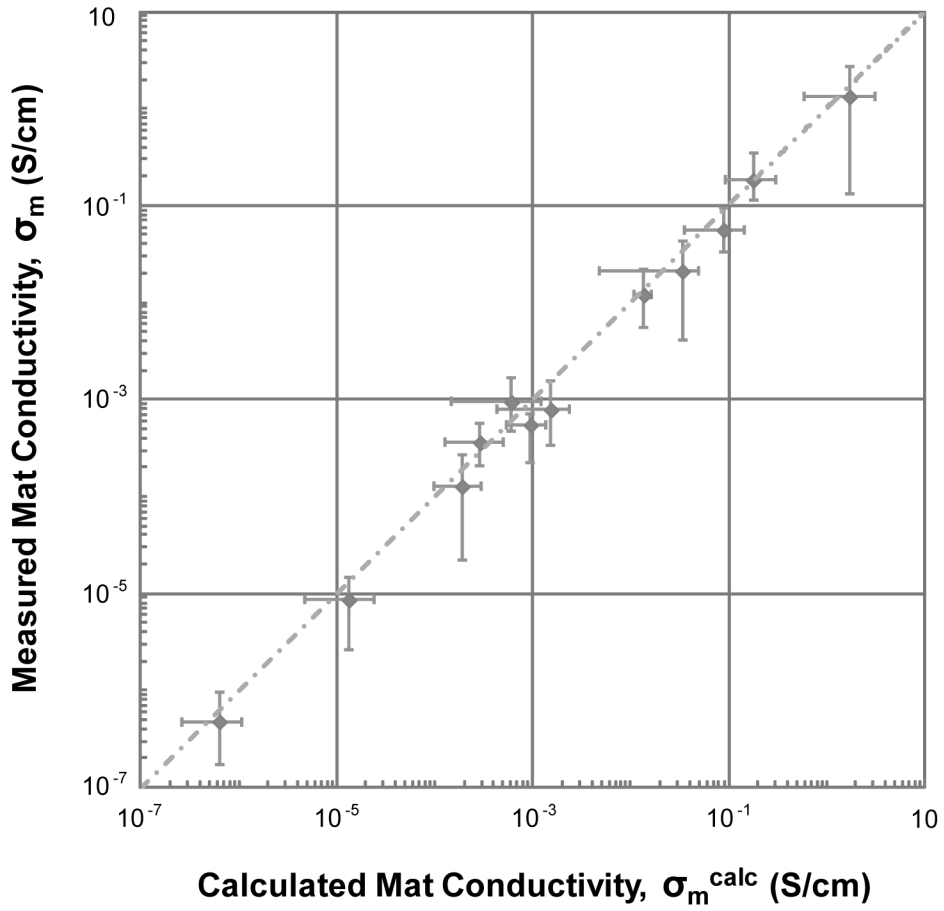

Figure 12 Parity plot of the experimentally-observed mat conductivity versus that calculated by the model for PAni-blend and PAni fibers

The most likely source of the discrepancy between the measured and calculated mat conductivities is the curvature of the fibers in the mat. As observed previously by Pai et al.,[31] the curvature (or "curl") of electrospun fibers in fiber mats tends to be more important for fibers of smaller diameter. In fiber mats

where the diameters of individual fibers are around several hundred nanometers, the average radius of curvature was found to be on the order of 10 to 100 μm, which is much smaller than the dimensions of the mat samples measured in this study. The net effect of fiber curvature is a longer conduction path from one electrode to the other, so the model based on straight fibers overestimates the mat conductivity slightly.

Another possible source of discrepancy is the neglect of conductive contacts between fibers. Fibers that do not provide a conductive path from one electrode to the other may nevertheless contribute to the mat conductivity measurement if they make conductive contact with another fiber that touches the other electrode. However, this effect would lead to the systematic underprediction of mat conductivity, which is not observed here.

CONCLUSION

We have fabricated electrospun fibers of PAni doped with an (nominally) equimolar amount of HCSA blended with PEO or PMMA over a range of compositions. Pure PAni/HCSA fibers were fabricated by co-axial electrospinning and subsequent removal of the PMMA shell by dissolution. A reliable method to characterize fiber conductivity using IDE has been developed and applied to electrospun conductive polymer nanofibers for the first time. The conductivities of the PAni-blend fibers are found to increase exponentially with the weight percent of doped polyaniline in the fibers, to as high as 50 ± 30 S/cm for as-electrospun fibers of 100% PAni/HCSA. This fiber conductivity was found to increase to 130 ± 40 S/cm with increasing molecular orientation, achieved through solid state drawing. Using a model that accounts for the effects of intrinsic fiber conductivity (including both composition and molecular orientation), mat porosity, and the fiber orientation distribution within the mat, calculated mat conductivities are obtained in quantitative agreement with the mat conductivities measured experimentally.

ACKNOWLEDGMENT

We thank Prof. K.K. Gleason, Prof. H.L. Tuller, and Prof. V. Bulovic for helpful discussions. We are grateful to Dr. Dimitrios Tzeranis for providing the MATLAB code to analyze SEM images for fiber orientation distributions. This research was supported by the U.S. Army through the Institute for Soldier Nanotechnologies (ISN), under contract ARO W911NF-07-D-0004.

REFERENCES

(1) Fridrikh, S.V.; Yu, J.H.; Brenner, M.P.; Rutledge, G.C. *Phys. Rev. Lett*. **2003,** *90*, 144502

(2) Shin, Y.M.; Hohman, M.M.; Brenner, M.P.; Rutledge, G.C. *Appl. Phys. Lett.* **2001,** *78*, 1149-1151

(3) Reneker, D.H.; Yarin, A.L.; Zussman, E.; Xu, H. *Adv. Appl. Mechanics* **2007,** *41*, 43-195

(4) Wang, X.Y.; Drew, C.; Lee, S.H.; Senecal, K.J.; Kumar, J.; Sarnuelson, L.A. *Nano Lett.* **2002,** *2*, 1273-1275

(5) Krupenkin, T.N.; Taylor, J.A.; Wang, E.N.; Kolodner, P.; Hodes, M.; Salamon, T. *Langmuir* **2007,** *23*, 9128-9133

(6) Hoth, C.N.; Choulis, S.A.; Schilinsky, P.; Brabec, C.J. *Adv. Mater*. **2007,** *19*, 3973-3978

(7) Salgado, A.J.; Coutinho, O.P.; Reis, R.L. *Macromol. Biosci.* **2004,** *4*, 743-765

(8) Schreuder-Gibson, H.L.; Truong, Q.; Walker, J.E.; Owens, J.R.; Wander, J.D.; Jones, W.E. *MRS Bulletin* **2003,** *28*, 574-578

(9) Ma, M.; Gupta, M.; Li, Z.; Zhai, L.; Gleason, K.K.; Cohen, R.E.; Rubner, M.F.; Rutledge, G.C. *Adv. Mater.* **2007,** *19*, 255-259

(10) Yu, J.H.; Fridrikh, S.V.; Rutledge, G.C. *Polymer* **2006,** *47*, 4789-4797

(11) Reneker, D.H.; Chun, I. *Nanotechnology* **1996,** *7*, 216-223

(12) Dong, H.; Nyame, V.; MacDiarmid, A.G.; Jones, W.E. *J. Polym. Sci. B* **2004,** *42*, 3934-3942

(13) Wei, M.; Lee, J.; Kang, B.; Mead, J. *Macromol. Rapid Commun*. **2005,** *26*, 1127-1132

(14) Zhu, Y.; Zhang, J.; Zheng, Y.; Huang, Z.; Feng, L.; Jiang, L. *Adv. Funct. Mater*. **2006,** *16*, 568-574

(15) Norris, I.D.; Shaker, M.M.; Ko, F.K.; MacDiarmid, A.G. *Synth. Metals* **2000,** *114*, 109-114

(16) Fryczkowski, R.; Kowalczyk, T. *Synth. Metals* **2009,** *159*, 2266-2268

(17) Ko, F.F.; MacDiarmid, A.G.; Norris, I.D.; Shaker, M.; Lec, R.M.. US Patent 7,264,762, Sep. 4, 2007

(18) Aussawasathien, D.; Dong, J.H.; Dai, L. *Synth. Metals* **2005,** *154*, 37-40

(19) Pomfret, S.J.; Adams, P.; Comfort, N.; Monkman, A.P. *Polymer* **2000,** *41*, 2265-2269

(20) Sun, Z.C.; Zussman, E.; Yarin, A.L.; Wendroff, J.H.; Greiner, A. *Adv. Mater.* **2003,** *15*, 1929-1932

(21) Yu, J.H.; Fridrikh, S.V.; Rutledge, G.C. *Adv. Mater.* **2004,** *16*, 1562-1566

(22) Shin, Y.M.; Hohman, M.M.; Brenner, M.P.; Rutledge, G.C. *Polymer* **2001,** *42*, 9955-9967

(23) Hohman, M.M.; Shin, Y.M.; Rutledge, G.C.; Brenner, M.P. *Phys. Fluids* **2001,** *13*, 2221-2236

(24) Li, D.; Wang, Y.; Xia, Y. *Nano Lett.* **2003,** *3*, 1167-1171

(25) Skotheim, T.A.; Elsenbaumer, R.L.; Reynolds, J.R., Eds., In *Handbook of Conducting Polymers*; Marcel Dekker: New York, 1998

(26) Wang, M.; Yu, J.H.; Kaplan, D.L.; Rutledge, G.C. *Macromolecules* **2006,** *39*, 1102-1107

(27) Trchova, M.; Zemek, J.; Stejskal, J. *Macromolecules* **1998,** *31*, 2218–2222f27

(28) Yu, Q.; Shi, M.; Deng, M.; Wang, M.; Chen, H. *Mat. Sci. Eng. B* **2008,** *150*, 70-76

(29) Pai, C.L.; Boyce, M.C.; Rutledge, G.C. *Polymer* **2011,** *52*, 2295-2301

(30) Jaehne B. In *Digital Image Processing*, 6th ed.; Springer: New York, 2005

(31) Pai, C.L.; Boyce, M.C., Rutledge, G.C. *Polymer* **2011,** *52*, 6126-6133

For Table of Contents use only

Electrical Conductivity of Electrospun Polyaniline and Polyaniline-Blend Fibers and Mats

Yuxi Zhang, Gregory C. Rutledge